ResearchGate

See discussions, stats, and author profiles for this publication at: https://www.researchgate.net/publication/281480855

# Conformational Identification and Phase Transition Behavior of Poly(trimethylene 2,6-naphthalate) α-Form Modification

**ARTICLE** *in* MACROMOLECULES · AUGUST 2015

Impact Factor: 5.8 · DOI: 10.1021/acs.macromol.5b01087

READS

23

**2 AUTHORS:**

Yongri Liang

Beijing Institute of Petrochemical Technology

**46** PUBLICATIONS **408** CITATIONS

SEE PROFILE

Han Sup Lee

Inha University

**33** PUBLICATIONS **533** CITATIONS

SEE PROFILE

Available from: Yongri Liang
Retrieved on: 25 January 2016

Macromolecules

Article

pubs.acs.org/Macromolecules

# Conformational Identification and Phase Transition Behavior of Poly(trimethylene 2,6-naphthalate) α-Form Modification

Yongri Liang*,† and Han Sup Lee‡

†College of Materials Science and Engineering, Beijing Key Laboratory of Special Elastomer Composite Materials, Beijing Institute of Petrochemical Technology, Beijing 102617, P. R. China

‡Department of Applied Organic Materials Engineering, INHA University, Incheon 402-751, Korea

Downloaded by BEIJING INST PETROCHEMICAL TECHLGY on August 31, 2015 | http://pubs.acs.org
Publication Date (Web): August 14, 2015 | doi: 10.1021/acs.macromol.5b01087

**ABSTRACT:** Poly(trimethylene 2,6-naphthalate) (PTN) is one of the 1,3-propanediol (PDO)-based aromatic polyesters which has potential applications for special barrier films and packaging due to its excellent oxygen and carbon dioxide gas barrier property. In this work, we investigated the chain conformation and phase transition behavior of poly(trimethylene 2,6-naphthalene) (PTN) α-form crystal with synchrotron wide- and small-angle X-ray scattering (WAXS and SAXS), attenuated total reflection Fourier transform infrared (ATR-FTIR) spectroscopy, and differential scanning calorimetry (DSC) methods. ATR-FTIR results showed that the infrared bands at 1327 and 987 $cm^{-1}$ were sensitive to PTN α-form crystalline phase and were assigned to *trans* conformers of trimethylene group, whereas the infrared bands at 1357 and 1372 $cm^{-1}$ were sensitive to PTN β-form crystalline phase and were assigned to *gauche* conformers of the trimethylene group. The results showed that the conformation of trimethylene glycol residue in PTN α-form crystalline phase adopted G′TTG or GTTG′ conformation. The DSC, WAXS, SAXS, and ATR-FTIR results indicate that the PTN α-form crystal undergoes structure changes at above 170 °C. We found that the PTN α-form crystal can transform to more stable crystalline phase (named as α′-form) by annealing. The crystal changes of PTN α-form crystal are associated with interchains rearrangement rather than with conformation changes of trimethylene glycol residue. The interchains rearrangement in PTN α-form crystalline phase may be caused by the internal force field change generated by the surface recrystallization process.

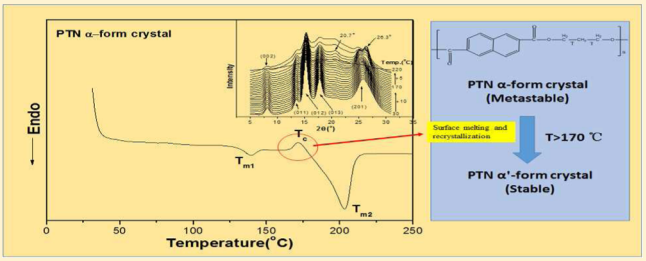


## INTRODUCTION

Nowadays, the major quantity of bio-based 1,3-propanediol (PDO) has achieved commercially viable products. It is possible to make bio-based polymers based on PDO. A major application of PDO is manufacturing poly(trimethylene terephthalate) (PTT) which is used for carpets and some industrial textile applications due to its excellent properties. Poly(trimethylene 2,6-naphthalate) (PTN) is another PDO-based aromatic polyester which has potential applications for special barrier films and packaging due to its excellent oxygen and carbon dioxide gas barrier property.[1] Even though several studies for PTN such as synthesis,[2] rheological properties,[3] fiber properties,[4] melt and crystallization behaviors,[5] crystal structural,[6] and surface-induced crystal orientation,[7] etc., have been reported so far, a fundamental understanding of structure formations of PTN is very limited for tailoring and optimization of their properties.

PTN has been reported to have two different crystalline modifications, α- and β-forms.[5] Jeong et al.[5] found that the PTN α- and β-form crystal formations depend on crystallization temperature. The PTN α-form crystal can be obtained below 140 °C of melt-crystallization temperatures, and the PTN β-form crystal can be obtained above 160 °C of melt-crystallization temperatures. Both PTN α- and β-form crystals can be obtained between 140 and 160 °C of melt-crystallization temperatures. The PTN α-form crystal can also be developed during cold-crystallization. The crystal structures of PTN have been first identified by Joeng et al.[8] The PTN α-form crystal is monoclinic with unit cell parameters of $a = 0.744$ nm, $b = 0.707$ nm, $c = 2.384$ nm, $\alpha = 90°$, $\beta = 90°$, and $\gamma = 81.6°$; the PTN β-form crystal is triclinic with unit cell parameters of $a = 0.467$ nm, $b = 0.701$ nm, $c = 2.218$ nm, $\alpha = 100.8°$, $\beta = 88.8°$, and $\gamma = 120.6°$. Joeng et al. also reported that the conformation of trimethylene unit and neighboring naphthalene units in the PTN β-form crystal adopted a *gauche/gauche* (GG) conformation and face-to-face type arrangement. For PTN α-form crystal, however, the detailed chain conformation has not been reported so far.

The crystallization and melting behaviors of PTN have been investigated by Jeong's[5] and Chuang's[9] groups; however, some of their results are incompatible. For example, Joeng et al. reported that the equilibrium melting temperatures of PTN α- and β-form crystals were 197 and 223 °C, respectively. They suggested that the crystal transition from α- to β-form may occur at 154 °C based on analysis of spherulitic growth rate of PTN using the second nucleation theory proposed by Laurizen

**Received:** May 20, 2015
**Revised:** August 10, 2015
**Published:** August 14, 2015

 © 2015 American Chemical Society 

DOI: 10.1021/acs.macromol.5b01087
*Macromolecules* 2015, 48, 5697−5705

Downloaded by BEIJING INST PETROCHEMICAL TECHLGY on August 31, 2015 | http://pubs.acs.org
Publication Date (Web): August 14, 2015 | doi: 10.1021/acs.macromol.5b01087

and Hoffman. Whereas Chuang et al.[9] reported that the both equilibrium melting temperatures of $\alpha$- and $\beta$-form crystals were 215 and 237 °C, respectively. They suggested the mechanism of $\alpha$- to $\beta$-crystal transformation which is a typical melting−recrystallization process based on heating of PTN $\alpha$-form crystal, i.e., first via surface melting of $\alpha$-lamellae and then the PTN chains near the boundaries of surviving $\alpha$-lamellae modify their conformation to form the $\beta$-crystal resulting in thickening lamellae. Nevertheless, the mechanism of PTN $\alpha$- to $\beta$-crystal transformation is still in doubt.

In general, the crystal modification transition of polymers is concomitant with chain conformation changes. Fourier transform infrared spectroscopy (FTIR) is typically sensitive to the conformation and local molecular environment of polymers. There are many examples where the crystal structure and crystallization process of various semicrystalline polymers have been investigated by the FTIR technique. Surprisingly, the FTIR studies of structure and conformation for PTN have not been reported so far.

Therefore, in order to more understand the structure changes of PTN $\alpha$-form crystal, we characterized the chain conformation of $\alpha$- and $\beta$-form crystals using FTIR technique and investigated structure and conformation changes of PTN $\alpha$-form crystal during heating process with *in situ* synchrotron small- and wide-angle X-ray scattering (SAXS and WAXS), differential scanning calorimetry, and FTIR methods.

## EXPERIMENTAL SECTION

**Materials and Samples Preparation.** PTN samples used in this study were synthesized with 1,3-propanediol and dimethyl-2,6-naphthalene dicarboxylate.[7,10] The intrinsic viscosity of PTN was 0.52 dL/g, which was measured in a mixed solvent of 1,1,2,2-tetrachloroethane and phenol (1/1, w/w) at 25 °C. The glass transition and melting temperature of PTN were 83 and 203 °C, respectively. To prepare the amorphous PTN samples, PTN chips were melted at 235 °C for 3 min on a hot presser to remove thermal history and then pressed, followed by quenched into ice water to obtain about 20 and 200 $\mu$m thicknesses of thin films. To prepare isothermally melt-crystallized samples, the melt-quenched PTN film were premelted at 235 °C for 3 min and then rapidly quenched to certain crystallization temperature to isothermally crystallize for 2 h.

**ATR-FTIR Measurements.** The attenuated total reflection Fourier transform infrared (ATR-FTIR) spectra were recorded by a Bruker IFS66v/s FTIR spectrometer with 2 $cm^{-1}$ of resolution and a variable angle ATR attachment (Nicolet Corp.). The angle of incidence ($\theta$) of the infrared radiation at the interface between the ATR crystal (ZnSe) and the polymer films was set to 45°. When mounting the sample on the ATR crystal, a torque wrench was used to maintain a constant pressure (40 oz./in.$^2$) to enhance the optical contact between sample and ATR crystal. It is because the samples used were somewhat thicker to be used for optimum transmission FTIR mode. In fact, thinner sample was hard to be prepared by melt-pressing method. The ATR-FTIR might be used without any significant errors to characterize the PTN crystalline phases in this work. In our case, the refractive index of amorphous PTN ($n_2$) is 1.64, the refractive index of ATR crystal (ZnSe) ($n_1$) is 2.4, and the incidence angle is 45°, so the penetration depth, $d_p$, at 1000 $cm^{-1}$ is calculated to be as 3.65 $\mu$m by eq 1.

$$d_p = \frac{\lambda}{2\pi(n_1^2 \sin^2\theta - n_2^2)^{1/2}} \quad (1)$$

**Synchrotron WAXS and SAXS.** The synchrotron wide- and small-angle X-ray scattering (WAXS and SAXS) patterns of annealed PTN samples were obtained at room temperature at 4C1 beamline in Pohang Accelerator Laboratory (PAL), Korea. The wavelength was 0.1608 nm, and a 2D CCD detector (1242 × 1152 pixels, 128.5 × 119.2 mm, Princeton Instrument Inc.) was used. *In situ* WAXS and SAXS experiments were carried out at the 4C2 beamline in Pohang Accelerator Laboratory (PAL), Korea. The wavelength was 0.154 nm, and a 2D detector (1242 × 1152 pixels, 128.5 × 119.2 mm, Princeton Instrument Inc.) was used. The samples were heated with lab-built temperature controllable hot stage by 10 °C/min. The SEBS (layer spacing is 32.5 nm) and silicon powder were used to calibrate the scattering vectors of SAXS and WAXS patterns, respectively.

**Crystallinity.** The crystallinity ($x_c$) was evaluated from WAXS data using the equation

$$x_c = A_{cr}/(A_{cr} + A_{am}) \quad (2)$$

Here, $A_{cr}$ and $A_{am}$ denote the total scattering intensities of crystalline and amorphous phases, respectively.

**SAXS Analysis.** The SAXS profiles were corrected to remove the air and the parasitic scattering before analysis. The one-dimensional correlation function (1DCF) was used to analyze the structure parameters of lamellar crystal such as long period, $L$, crystalline phase thickness, $l_c$, and amorphous phase thickness, $l_a$.[11−13] The normalized 1DCF was as follows:

$$\gamma(z) = r(z)/r(0) = \int_0^\infty I(q)q^2 \cos(qz)\, dq \quad (3)$$

where $z$ is the axis normal to the layer faces in the lamellar stack, $r(0) = Q = \int_0^\infty I(q)q^2\, dq$, $q = 4\pi \sin(\theta)/\lambda$, $\lambda$ is the wavelength of the X-ray source, and $2\theta$ is the scattering angle. Because the experimentally accessible $q$ range is finite, the extrapolation of the scattered intensity to both lower side and higher side $q$ range is necessary. The extension of the scattering intensity over the higher $q$ range (0.11−0.16 Å$^{-1}$) is performed using Porod's law,[14] and the extrapolation to zero $q$ data is carried out by the curve fitting of the intensity at a low $q$ range (0.00−0.015 Å$^{-1}$) using the Debye−Bueche model.[14] The long period $L$ is obtained from the first peak maximum $\gamma(z)$ value of $\gamma(z)$ versus $z$ plot. And the thickness of one layer $l_1$ in the lamellar stack (crystal or amorphous layer) is estimated from the intersection point of the linear line of absolute maximum slope and the horizontal line containing the lowest correlation function value in the plot of $\gamma(z)$ versus $z$ as shown in Figure 1. The other layer thickness ($l_2$) can be obtained from $L$ and

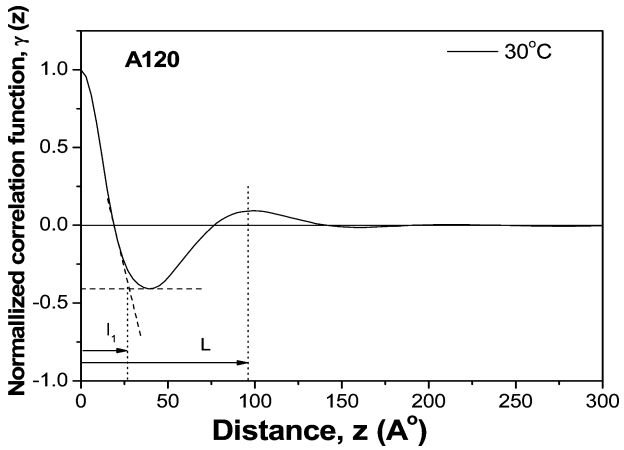


**Figure 1.** Illustration of the long period, $L$, and layer thickness, $l_1$, obtained from normalized 1D correlation function. The long period, $L$, can be obtained from first maximum value of $\gamma(z)$, and the $l_1$ can be obtained from first minimum value. The A120 sample is prepared by isothermal melt-crystallization at 120 °C for 2 h.

$l_1$; $l_2 = L - l_1$. $l_1$ can be assigned to the thickness either of lamellar crystal or of the amorphous layer in the lamellar stacks formed in polymer sample. The linear crystallinity $x_l$ ($x_l = l_c/L$) can be obtained by ratio of lamellar crystal thickness to the long period. In the present study, $l_1$ value is found to be smaller than $l_2$. The crystallinity ($x_c$) obtained with the WAXS pattern was about 0.4. On the basis of the correlation function analysis and crystallinity by WAXS ($x_l \geq x_c$), we were able to assign the $l_2$ value to the lamellar crystal layer thickness



DOI: 10.1021/acs.macromol.5b01087
*Macromolecules* 2015, 48, 5697−5705

and $l_1$ to the amorphous layer thickness. The invariant $Q$, which represents the total integrated scattering, was obtained from the Lorentz corrected SAXS profile using the equation

$$Q = \int_0^\infty I(q)q^2 \, dq \tag{4}$$

The invariant value is related to electron density difference between the crystalline and noncrystalline region $(\rho_c - \rho_a)$ and the amount of two phases as shown in the equation

$$Q \propto x_s x_l (1 - x_l)(\rho_c - \rho_a)^2 \tag{5}$$

where $x_s$ is the volume fraction of lamellar stacks and $x_l$ is the linear crystallinity within lamellar stack ($x_l = l_c/L$). The $\rho_c$ and $\rho_a$ are the densities of the crystalline and the amorphous regions, respectively. The volume crystallinity of the overall sample is given by $x_s \cdot x_l$.

**Differential Scanning Calorimetry (DSC).** DSC thermographs were obtained with a Shimadzu DSC-50 using 10 °C/min heating rate under the dry nitrogen gas purging.

## RESULTS AND DISCUSSION

**Conformation Identification of PTN $\alpha$- and $\beta$-Form Crystals.** In order to obtain amorphous $\alpha$-form crystal and $\beta$-form crystal samples of PTN, the samples were prepared by melt-quenching (melt-quenched sample), isothermal melt-crystallization at 120 °C for 2 h (A120 sample), and isothermal melt-crystallization at 180 °C for 2 h (A180 sample), respectively. The crystal structure of PTN samples were identified by WAXS as shown in Figure 2A. The amorphous diffraction peak was observed in the melt-quenched PTN sample, and PTN $\alpha$- and $\beta$-form crystals diffraction peaks are observed in the A120 and A180 samples, respectively. For example, the diffraction peaks at 8.08°, 13.15°, 14.74°, 17.21°, and 24.75° in the WAXS profile of A120 sample can be assigned to (002), (011), (012), (013), and (201) crystal planes of PTN $\alpha$-form crystal, respectively. And the diffraction peaks at 8.37°, 15.39°, 18.99°, 20.18°, 24.52°, and 26.48° in the WAXS profile of A180 sample can be assigned to (002), (010), (012), $(\bar{1}11)$, $(1\bar{1}2)$, (102), and (104) crystal planes of PTN and $\beta$-form crystal, respectively. Accordingly, the melt-quenched A120 and A180 samples represent the amorphous, $\alpha$-form and $\beta$-form crystalline phases, respectively.

Therefore, on the basis of the ATR-FTIR spectrum of A120, we can identify that the bands at 1465, 1325, 1042, 987, 942, and 819 $cm^{-1}$ are sensitive to PTN $\alpha$-form crystalline phase. Similarly, on the basis of the ATR-FTIR spectrum of A180, we can also identify that the bands at 1464, 1372, 1339, 1186, 1133, 1093, 1045, 968, 950, and 829 $cm^{-1}$ are sensitive to PTN $\beta$-form crystalline phase. The characteristic infrared bands of PTN $\alpha$- and $\beta$-form crystals showed a significant difference. It means that PTN $\alpha$- and $\beta$-form crystals have very different chain conformations.

Joeng et al.[8] reported that the chain conformation of trimethylene glycol residue in the PTN $\beta$-form crystalline phase adopted trans−gauche−gauche−trans (TGGT) conformation, and the neighboring naphthalene units in the PTN $\beta$-form crystallographic unit cell are arranged as face-to-face type. In contrast with PTN $\beta$-form crystalline phase, the conformation of trimethylene glycol residue in the PTN $\alpha$-form crystalline phase has not been reported in detail so far.

The conformations of trimethylene group of PTN crystalline phases can be detected in the infrared regions of 1500−1300 and 1000−800 $cm^{-1}$, and the conformations of naphthalene ring groups of the PTN crystalline phases can be detected in the infrared absorption region of 1300−1000 $cm^{-1}$. For the

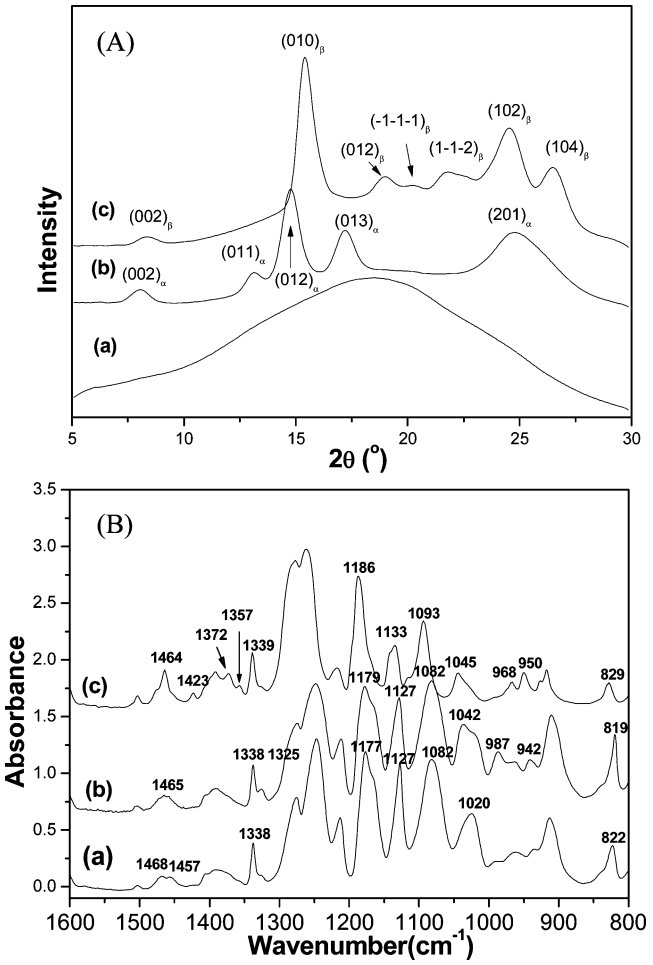


**Figure 2.** (A) WAXS profiles and (B) ATR-FTIR spectra of PTN samples with various thermal histories: (a) melt-quenched sample, (b) isothermal melt-crystallization at 120 °C for 2 h (sample A120), and (c) isothermal melt-crystallization at 180 °C for 2 h (sample A180).

PTN $\beta$-form crystal, the infrared bands at 1357, 1372, 1423, and 1464 $cm^{-1}$ are sensitive to PTN $\beta$-form crystalline phase as shown in Figure 2B(c). In addition, the bands at 1468 and 1457 $cm^{-1}$ are assigned to $CH_2$ bending vibration modes.[15] Accordingly, we can determine that the bands at 1357, 1372, 1423, and 1464 $cm^{-1}$ are associated with gauche conformers because the trimethylene glycol residue in the PTN $\beta$-form crystalline phase adopted TGGT conformation. A similar TGGT conformation of trimethylene glycol residue has been observed in the crystalline phase of poly(trimethylene terephthalate) (PTT).[16] In the case of PTT, the infrared bands at 1358 and 1465 $cm^{-1}$ are sensitive to the gauche conformers.[17−19]

The bands at 1465 and 1325 $cm^{-1}$ are sensitive to PTN $\alpha$-form crystalline phase as shown in Figure 2B(b). It indicates that the conformation of trimethylene glycol residue in PTN $\alpha$-form crystalline phase is completely different with that in PTN $\beta$-form crystalline phase. By comparison between the ATR-FTIR spectrum of PTN amorphous (in the melt-quenched sample) and $\alpha$-form crystalline phases (A120 sample), we can find that the absorbance of band at 1327 $cm^{-1}$ is enhanced after formation of $\alpha$-form crystals, and its position is shifted from 1327 to 1325 $cm^{-1}$. The band at 1325 $cm^{-1}$ is attributed to $CH_2$ wagging vibration mode. The similar band at 1326 $cm^{-1}$ was observed in the PTT amorphous phase and was assigned to

Downloaded by BEIJING INST PETROCHEMICAL TECHLGY on August 31, 2015 | http://pubs.acs.org
Publication Date (Web): August 14, 2015 | doi: 10.1021/acs.macromol.5b01087



DOI: 10.1021/acs.macromol.5b01087
Macromolecules 2015, 48, 5697−5705

trans conformer. Similarly, we suggest that the band at 1325 $cm^{-1}$ is sensitive to PTN $\alpha$-form crystalline phase and is associated with trans conformer. In addition, the band at 987 $cm^{-1}$ is also sensitive to PTN $\alpha$-form crystalline phase and is assigned to $CH_2$ rocking vibration mode. The similar band at 987 $cm^{-1}$ is observed in the crystalline phases of poly(ethylene 2,6-naphthalate) (PEN)[15] and poly(buthylene 2,6-naphthalate) (PBN).[20] In the both cases of PEN and PBN, the band at 987 $cm^{-1}$ is associated with trans conformers of methylene group. Therefore, we could be able to conclude that the conformation of trimethylene group in PTN $\alpha$-form crystalline phase adopted trans conformer.

The band at 1042 $cm^{-1}$ is sensitive to PTN $\alpha$-form crystalline phase and is assigned to vibration of glycol linkage of C−O with gauche (G) conformer. Similar bands are also reported in the PEN and PBN.[15] It means that the trimethylene glycol residue in PTN $\alpha$-form crystalline phase may adopt gauche−trans−trans−gauche conformation. The trimethylene glycol residue in PTN can adopt TTTT, G′TTG′, GTTG (where G is 60° and G′ is −60°), G′TTG, and GTTG′ conformations. The molecular models of PTN chain with various conformation of trimethylene glycol residue are simulated using a commercial software Materials Studio (version 7.0). The simulation results showed that the PTN chain has extended shape for TTTT conformation, helical shape for GTTG and G′TTG′ conformations, and Z shape for G′TTG and GTTG′ conformations as shown in Figure 3. The PTN chain with G′TTG or GTTG′ conformation is more extended than that with the GTTG or G′TTG′ conformation. In the view of chain packing in the crystal unit cell, the PTN chains with GTTG and G′TTG′ conformations are impossible to pack into crystal unit cell due to large space barrier. Therefore, the PTN $\alpha$-form crystal might have one of TTTT, G′TTG, or GTTG′ conformation. Based on the crystal structure modeling of PTN $\alpha$-form crystal (using a commercial software Materials Studio, version 7.0), the length of $c$-axis in PTN crystal was calculated as 2.602 nm for TTTT conformation, 2.483 nm for G′TTG conformation, 2.389 nm for GTTG′ conformation, and 2.218 nm for TGGT conformation after energy-minimizing calculations of crystal structure. The COMPASS force field[21] and the Ewald summation method[22,23] were used in energy-minimizing calculations of crystal structure. The $\beta$-form crystal structure was built initially based on Jeong et al.'s work;[8] then the chain conformation of trimethylene glycol residue in the PTN was varied to specific conformation manually. For example, to obtain a chain of G′TTG, the four torsional angles of the four successive bonds were set to be −60°, 180°, 180°, and 60°. The crystal structure parameters of PTN $\alpha$-form crystal are reported by Jeong et al.[8] as $a$ = 0.744 nm, $b$ = 0.707 nm, $c$ = 2.384 nm, $\alpha$ = 90°, $\beta$ = 90°, and $\gamma$ = 81.6°. In the view of the length of $c$-axis in the unit cell, the G′TTG or GTTG′ conformation of trimethylene glycol residue in the PTN $\alpha$-form crystalline phase are more reasonable. The crystallographic parameter showed that the length of $c$-axis in PTN $\alpha$-form crystal ($c$ = 2.384 nm) is larger than that in the PTN $\beta$-form crystal ($c$ = 2.218 nm).[8] It provides more evidence for the conformation of trimethylene glycol residue in PTN $\alpha$-form crystalline phase, which might adopt G′TTG or GTTG′ conformation. From the crystallization kinetics view, the extended chain (TTTT) may not be easily incorporated into the crystalline phase during melt crystallization. On the basis of FTIR and simulation results, we suggest that the conformation of trimethylene glycol residue in PTN $\alpha$-form crystalline phase adopts G′TTG or GTTG′ conformation.

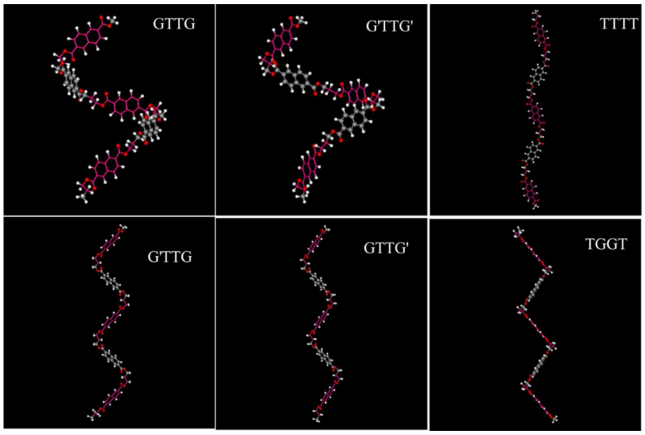


**Figure 3.** Molecular models of trimethylene glycol residue in the PTN chain with various conformations.

The conformations of naphthalene ring in the PTN $\alpha$- and $\beta$-form crystals could be analyzed with the infrared absorption region of 1300−1000 $cm^{-1}$. The bands at 1128 and 1177 $cm^{-1}$ were sensitive to the PTN amorphous phase as shown in the Figure 2B(a). The bands at 1128 and 1177 $cm^{-1}$ have been assigned to the naphthalene ring C−H in-plane vibration modes. It was found that the bands at 1128 and 1177 $cm^{-1}$ were almost uninfluenced upon the formation of PTN $\alpha$-form crystals. However, those were significantly shifted to 1134 and 1186 $cm^{-1}$ after formation of PTN $\beta$-form crystals as shown in Figure 2B(b,c). Those results indicate that packing arrangement of naphthalene units in PTN $\alpha$-form crystalline phase is somewhat different with that in PTN $\beta$-form crystalline phase. It may be due to the G′TTG conformation of trimethylene glycol residue in the PTN chain hindering the face-to-face arrangement. Compared with the $\beta$-form crystal, the PTN $\alpha$-form crystal is thermodynamically less stable possibly due to high packing energy.

**Thermal Behaviors of PTN $\alpha$-Form Crystal.** Figure 4 shows the DSC thermograms of A120, A180, and A120/180 samples obtained during heating process. The A120/180 sample was prepared by isothermal crystallization of A120 sample at 180 °C for 2 h. In the DSC thermogram of A120 sample, a small exothermic peak ($T_c$) was observed at 171.4 °C before the melting peak ($T_{m3}$) appears at 203.4 °C. It implies that structure change of PTN $\alpha$-form crystal occurred at just above 170 °C during heating process. If the A120 sample was annealed at 180 °C (A120/180), the exothermic peak, $T_c$, was not observed and a large melting peak ($T_{m2}$) appeared at 192.3 °C. In contrast with A120 and A120/180 samples, the A180 sample showed three melting peaks ($T_{m1}$, $T_{m2}$, and $T_{m3}$) at 188.6, 198.9, and 207.7 °C, respectively. Accordingly, we can deduce that the PTN $\alpha$-form crystal was transformed to become more stable crystal structure at above 170 °C, which is different from $\beta$-form crystal. The PTN $\alpha$-form crystal exists as a metastable state at this temperature.

**Structure Change of PTN $\alpha$-Form Crystal.** Figure 5 shows the WAXS profiles of sample A120 obtained at various temperatures during heating process. The WAXS profile of sample A120 showed PTN $\alpha$-form crystal at 30 °C. When the temperature increased to above 170 °C, "new" diffraction peaks appeared at around 20.7° and 26.8°, and their intensities were

Downloaded by BEIJING INST PETROCHEMICAL TECHLGY on August 31, 2015 | http://pubs.acs.org
Publication Date (Web): August 14, 2015 | doi: 10.1021/acs.macromol.5b01087



DOI: 10.1021/acs.macromol.5b01087
Macromolecules 2015, 48, 5697−5705

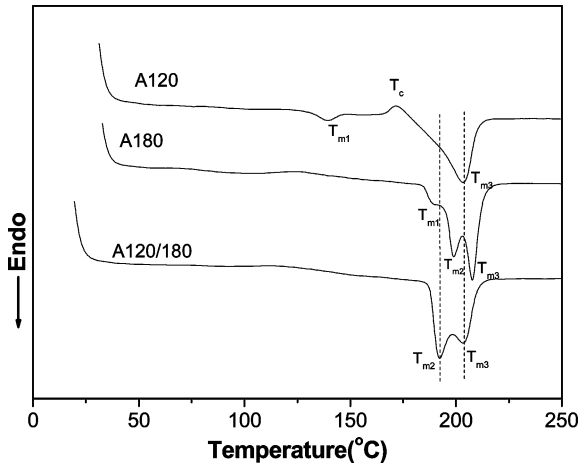


**Figure 4.** DSC thermograms of A120, A180, and A120/180 samples obtained during heating processes with 10 °C/min of heating rate. The A120 and A180 samples were prepared by isothermal melt-crystallization of melt-quenched PTN films at 120 and 180 °C for 2 h, respectively, and the A120/180 sample was prepared by annealing A120 at 180 °C for 2 h.

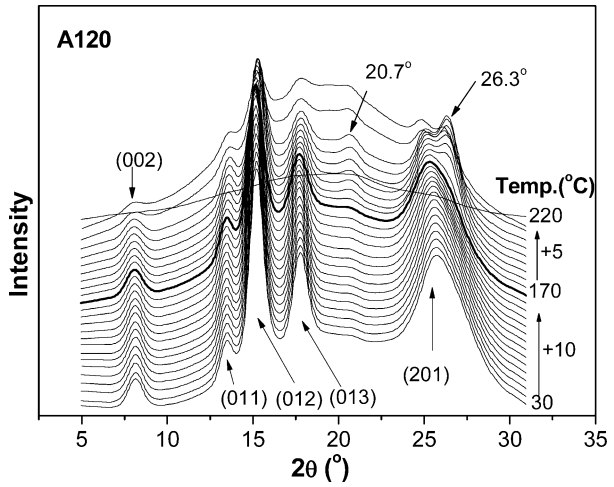


**Figure 5.** WAXS profiles of A120 sample obtained at different temperatures during heating process. The A120 sample was prepared by isothermal melt-crystallization of melt-quenched PTN film at 120 °C for 2 h.

grown up with increasing temperature until before melting, while other diffraction peaks at 8.08°, 13.15°, 14.74°, and 17.21° did not show any significant changes. In the WAXS profile of A120/180 sample, the "new" diffraction peaks at 20.7° and 26.8° could be obviously observed in Figure 6. The structure changes of PTN $\alpha$-form observed by WAXS are consistent with that observed by DSC. Chuang et al.[9] observed some diffraction peaks of $\beta$-form crystal when the $\alpha$-form crystal was heated at temperature above 170 °C. They explained that the part of $\alpha$-form crystal may be transformed into the $\beta$-form crystal during the heating process. Chuang et al.[9] noticed that the WAXS profile measured during the $\alpha$-form to $\beta$-form crystal transformation is different from that of the coexistence of $\alpha$- and $\beta$-crystals. In our work, however, we did not observe PTN $\beta$-crystal diffraction peaks when the PTN $\alpha$-form crystal was heated or annealed at above 170 °C of temperature. On the basis of the DSC and WAXS results, we suggest that the PTN $\alpha$-form crystal might be transformed to

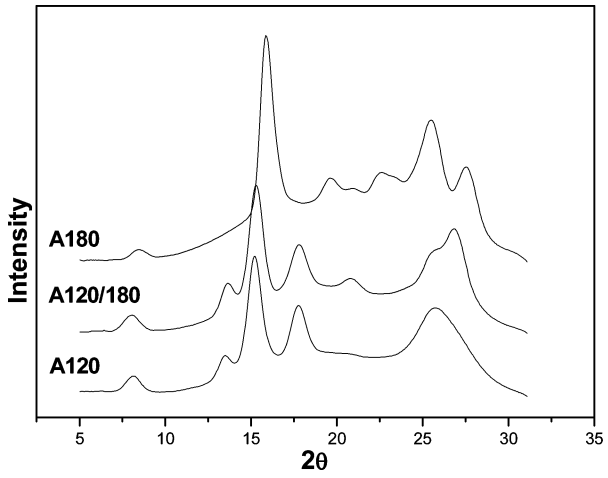


**Figure 6.** WAXS profiles of A120, A180, and A120/180 samples obtained at room temperature. The A120 and A180 samples were prepared by isothermal melt-crystallization of melt-quenched PTN films at 120 and 180 °C for 2 h, respectively, and the A120/180 sample was prepared by annealing A120 at 180 °C for 2 h.

more stable crystal state (called as $\alpha'$-form crystal) at above 170 °C. However, the $\beta$-form crystal was not observed during heating of PTN $\alpha$-form crystal.

**Crystal Morphology Changes of PTN $\alpha$-Form Crystal.** The crystal morphology changes of PTN $\alpha$-form crystal during heating process was observed by SAXS. As shown in Figure 7,

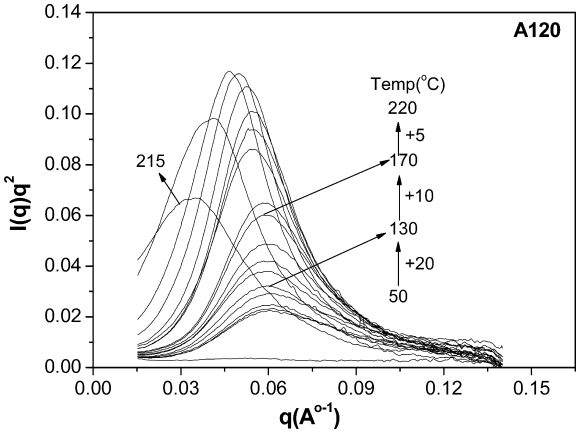


**Figure 7.** SAXS profiles of A120 sample obtained at different temperatures during heating process. The A120 sample was prepared by isothermal melt-crystallization of melt-quenched PTN films at 120 °C for 2 h.

the scattering vector of maximum intensity, $q_{max}$, almost remains constant in the temperature range of 50–170 °C. When the temperature increased to above 170 °C, the $q_{max}$ shifts to lower value. It means that the long period ($L_B = 2\pi/q_{max}$) is increased with increasing the temperature at above 170 °C. The detailed temperature dependence of the lamellar structure parameters such as long period ($L$), lamellar crystal thickness ($l_c$), and amorphous layer thickness ($l_a$) were obtained from one-dimensional correlation function, and the results are displayed in Figure 8. The temperature dependence of lamellar structure parameters can be divided into four regions (A to D) as shown in Figure 8. In the region A (30–130 °C), the values of $L$ (or $L_B$), $l_c$, and $l_a$ remain almost

Downloaded by BEIJING INST PETROCHEMICAL TECHLGY on August 31, 2015 | http://pubs.acs.org
Publication Date (Web): August 14, 2015 | doi: 10.1021/acs.macromol.5b01087



DOI: 10.1021/acs.macromol.5b01087
*Macromolecules* 2015, 48, 5697–5705

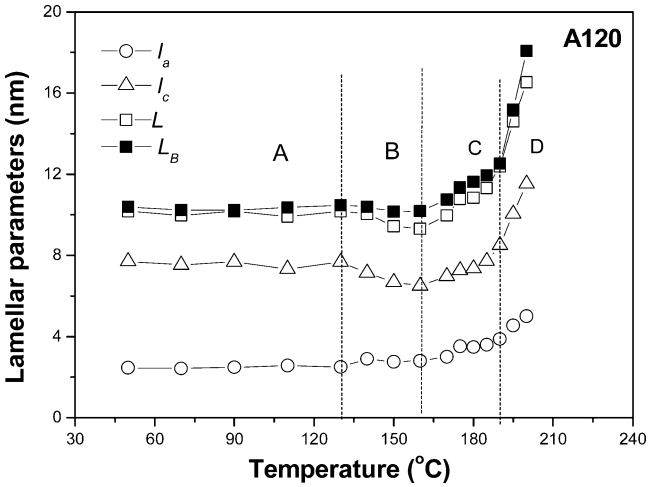


**Figure 8.** Long period ($L$ and $L_B$), lamellar crystal thickness ($l_c$), and amorphous layer thickness ($l_a$) of A120 sample obtained at different temperature during heating process. The A120 sample was prepared by isothermal melt-crystallization of melt-quenched PTN films at 120 °C for 2 h.

constant with the increasing temperature. In region B (130–160 °C), the values of $L$ (or $L_B$) and $l_c$ are slightly decreased with increasing temperature, whereas the $l_a$ is slightly increased. For example, the thickness of lamellar crystal decreased from 7.7 to 6.5 nm when the temperature increased from 130 to 160 °C (16% decrease); meanwhile, the crystallinity ($x_c$) by WAXS decreased from 0.39 to 0.30 (23% decrease). In addition, the linear crystallinity ($x_l$) by SAXS and invariant ($Q$) were decreased and increased with increasing temperature in the region B, respectively. In the DSC thermorgam of A120, a small melting peak was observed at 139.3 °C. Accordingly, the change of lamellar structure and crystallinity might be related with to the melting behavior of secondary PTN $\alpha$-form crystal. In the third temperature region, C (170–195 °C), the $L$ (or $L_B$) and $l_c$ values are increased with increasing temperature, whereas crystallinity ($x_c$) is kept almost constant. In the DSC thermogram of A120, a small exothermal peak was observed at 171.4 °C. Furthermore, the invariant is increased with increasing temperature as shown in Figure 9.

The structure changes of PTN $\alpha$-form crystal in the temperature region of B in Figure 8 seems to be related to the melting of secondary PTN $\alpha$-form crystals as shown with the DSC thermogram (Figure 4). The secondary crystals seems to be formed during secondary crystallization process. To explain the morphology change of PTN $\alpha$-form in the regions of B, a concrete morphological model that might be consistent with the experimental observations seems to be necessary for this work. In general, several morphological models for the lamellar structure have been proposed thus far to explain the SAXS results. Those are (1) single thin lamellar insertion model,[24,25] (2) thin lamellar stack insertion model,[26] and (3) short-range-ordered structure model.[27]

In the first model (single thin lamellar insertion model), secondary crystallization generates single thin lamellae in the amorphous layers of the lamellar stacks formed during primary crystallization. Therefore, the thicknesses of the lamellar and amorphous layers in the lamellar stack formed during primary crystallization remain constant throughout the secondary crystallization process. Thus, the average crystallinity should increase as the secondary crystallization proceeds, and the average lamellar thicknesses should decrease. In the second model (thin lamellar stack insertion model), (a) the secondary crystallization process involves the formation of thin lamellar stacks between the lamellar stacks already formed during primary crystallization, and (b) the lamellar thickness in the lamellar stacks formed during secondary crystallization is smaller than that of the lamellar stacks formed during primary crystallization. Thus, the average lamellar thickness decreases with time when secondary crystallization takes place, which means that the thinning of the average lamellar thickness occurs during the entire secondary crystallization process. (3) The short-range ordered structure model has been proposed by Ree et al. In this model, the secondary crystallization involves the formation of short-range molecular order in the amorphous layers of the lamellar stacks as well as in the amorphous regions between the lamellar stacks. This short-range ordered structure, which is likely a type of single thin lamella, thin lamellae, or

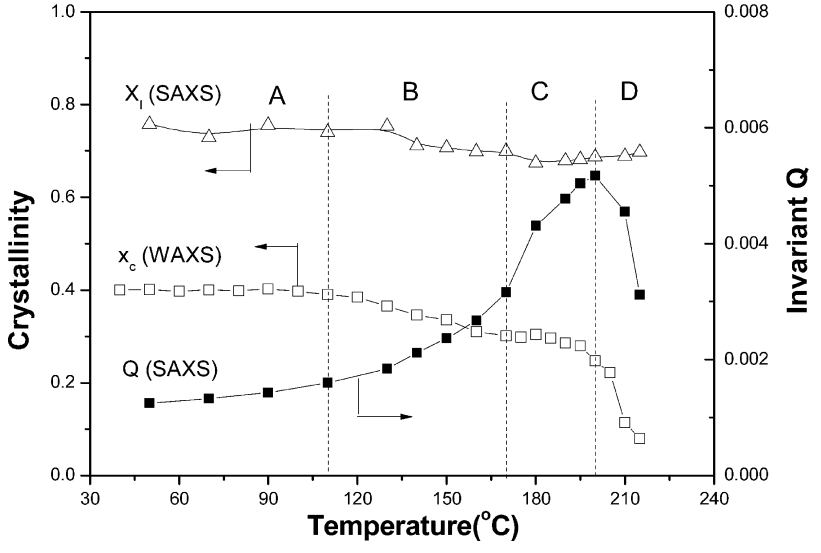


**Figure 9.** Crystallinity ($x_c$), linear crystallinity ($x_l$), and invariant ($Q$) of A120 obtained at different temperatures by SAXS and WAXS during heating process. The A120 sample was prepared by isothermal melt-crystallization of melt-quenched PTN films at 120 °C for 2 h.

Downloaded by BEIJING INST PETROCHEMICAL TECHLGY on August 31, 2015 | http://pubs.acs.org
Publication Date (Web): August 14, 2015 | doi: 10.1021/acs.macromol.5b01087



DOI: 10.1021/acs.macromol.5b01087
*Macromolecules* 2015, 48, 5697–5705

fringed micelle-like order, has a lower electron density than the lamellar crystal formed by primary crystallization.

The first and second models cannot explain our SAXS results because the lamellar thickness and crystallinity of PTN $\alpha$-form are decreased after melting of the secondary crystals. If the short-range ordered secondary crystals formed at the interphase between lamellar crystal and amorphous layers (i.e., the surface of lamellar crystal) in the lamellar stack during secondary crystallization, the lamellar thickness and crystallinity should be decreased by melting of secondary crystals. The abrupt increase of the invariant value in the region B (Figure 9) can be successfully interpreted by increase of the electron density difference between the crystal and amorphous layers after melting of the short-range ordered secondary crystals of lower electron density.

Therefore, we propose that the morphological changes in temperature region of B are due to the melting short-range ordered secondary crystals at interphase between primary lamellar crystalline and amorphous layers. Furthermore, the SAXS and WAXS results indicate that the structure changes of PTN $\alpha$-form crystal is caused by the recrystallization process at the crystal surface.

**Conformation Changes of PTN $\alpha$-Form Crystal.** In order to understand the structure change PTN $\alpha$-form crystal at the molecular level more clearly, we obtained the ATR-FTIR spectrum of A120 and A120/180 samples as shown in Figure 10. The bands at 1327 and 988 $cm^{-1}$ are sensitive to PTN $\alpha$-form crystalline phase as shown in spectrum of A120; however, those bands were shifted to 1323 and 984 $cm^{-1}$ after annealing at 180 °C as shown in the FTIR-ATR spectrum of A120/180. The peaks at 1323 and 984 $cm^{-1}$ are associated with vibrations of trimethylene group. Anomalous band shifts of some specific infrared bands have also been observed in several polymers such as t-POM,[28,29] o-POM,[30] PEO,[30] PTFE,[31] and PLLA.[32] For the anomalous band-shift phenomenon, some mechanisms have been proposed. Fawcett[33] ascribed the spectral change to different intermolecular forces caused by different chain packing. Tanabe and Shimomura[29] tried to interpret this phenomenon based on the induced dipole moment interactions. Kobayashi and Sakashita[30] interpreted quantitatively in terms of the transition dipole−dipole coupling theory developed initially by Hexter.[34] Kobayashi and Sakashita[30] summarized the common features of the remarkable spectral changes in the crystalline linear polymers of t-POM, o-POM, and PEO and described the reasons of band shifts as follows: (1) the anomalous band shifts were observed only for the infrared-active parallel bands, (2) the magnitude of the shift was proportional to the oscillator strength of the band, (3) the overtones of the parallel fundamental bands did not show such a remarkable shift, and (4) the appearance of the high-frequency bands in folded-chain crystal (FCC) was ascribed not to the folded molecular structure, but to the lamellar-type crystal morphology. In our case, the band shifting of 1327 and 988 $cm^{-1}$ is associated with the structure changes of PTN $\alpha$-form crystal during heating process or annealing. The band at 1326 $cm^{-1}$ has been assigned to $CH_2$ wagging vibration mode with trans conformation. The band at 988 $cm^{-1}$ has been assigned to trans glycol segment vibration mode. Both bands of 1327 and 988 $cm^{-1}$ showed parallel dichroism. Therefore, the peak shifts of bands at 1327 and 988 $cm^{-1}$ can be explained by enhanced interactions of intermethylene groups. It means that the interaction of intermethylene groups in PTN $\alpha'$-form crystalline phase is stronger than that in $\alpha$-form crystalline

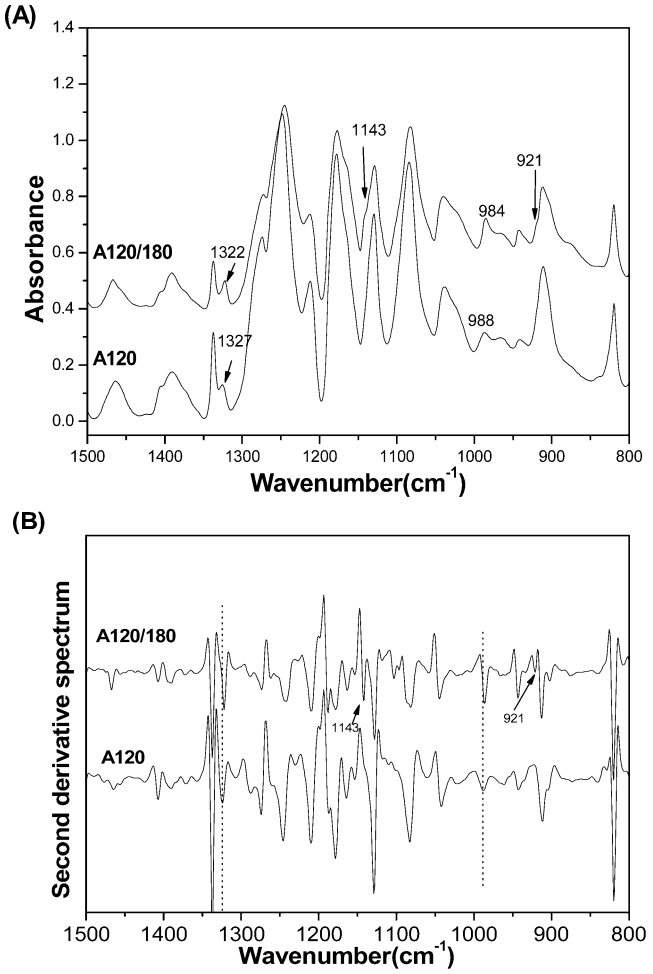


**Figure 10.** (A) FTIR-ATR and (B) second-derivative spectra of A120 and A120/180 samples obtained at room temperature. The A120 sample was prepared by isothermal melt-crystallization of melt-quenched PTN film at 120 °C for 2 h, and the A120/180 sample was prepared by annealing A120 at 180 °C for 2 h.

phase. In addition, we also observed new peaks appeared at 1143 and 921 $cm^{-1}$ in the ATR-FTIR spectrum of A120/180 as shown in Figure 7A,B. The peaks at 1143 and 921 $cm^{-1}$ have been assigned to C−H in-plane and C−H out-of-plane vibrations of naphthalene ring, respectively.[15] It indicates that the interaction of inter-naphthalene groups in PTN $\alpha'$-form crystalline phase is also stronger than that in $\alpha$-form crystalline phase. It also means that the chains in the PTN $\alpha'$-form crystalline phase is more compactly packed in the unit cell than that in $\alpha$-form crystalline phase.

The structure parameters of $a$, $b$, and $c$ in PTN $\alpha$-form crystal were calculated from the diffraction peaks of (201), (012), and (002), respectively. Figure 11 shows that the lengths of $b$-axis significantly decreased in the temperature region of C (170−195 °C) during heating process of PTN $\alpha$-form crystal. The length of $b$-axis in the crystal reflects the distance of interchains. It demonstrates that the distance of interchains in the PTN $\alpha'$-form crystal is shorter than that in PTN $\alpha$-form crystal. The surface melting and recrystallization process appears to generate internal stretching force[35] that causes the crystal transformation. On the basis of the DSC, WAXS, SAXS, and ATR-FTIR results, we concluded that the PTN $\alpha$-form crystal might be transformed to more stable $\alpha'$-form crystal by heating at temperature above 170 °C. The structure changes of PTN $\alpha$-

Downloaded by BEIJING INST PETROCHEMICAL TECHLGY on August 31, 2015 | http://pubs.acs.org
Publication Date (Web): August 14, 2015 | doi: 10.1021/acs.macromol.5b01087



DOI: 10.1021/acs.macromol.5b01087
Macromolecules 2015, 48, 5697−5705

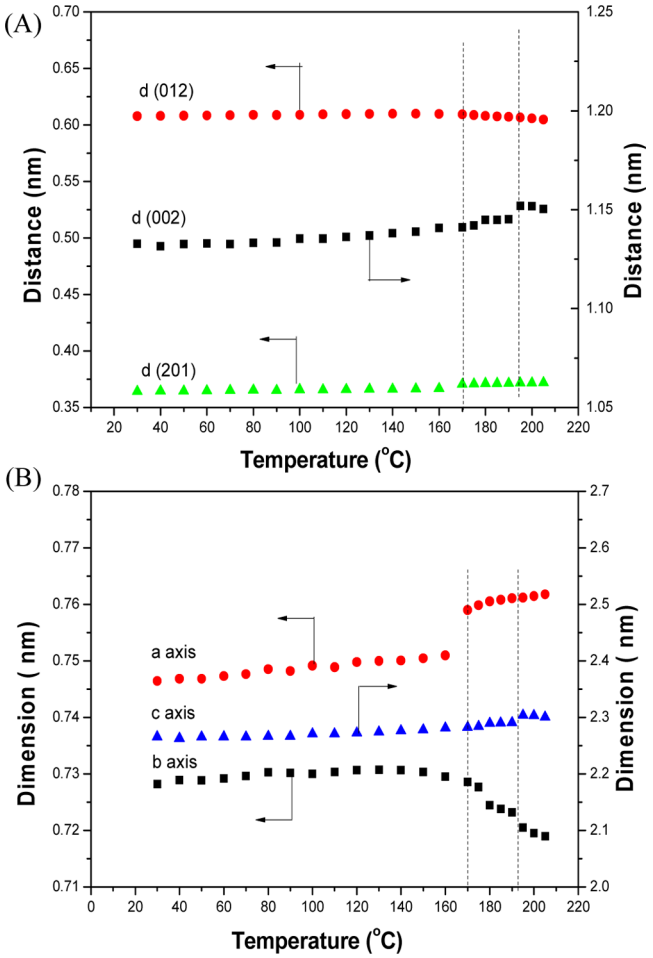


**Figure 11.** Temperature dependence of (A) interplane distance of (012), (201), and (002) planes and (B) the lengths of *a*-, *b*-, and *c*-axes in the PTN $\alpha$-form crystal calculated from Figure 5.

form PTN seems to be associated with interchains rearrangement caused by internal force field change which was generated by the surface recrystallization process.

## CONCLUSIONS

In this work, we identified the chain conformation of PTN $\alpha$- and $\beta$-form crystals by FTIR spectroscopy. The infrared bands at 1327 and 987 $cm^{-1}$ sensitive to PTN $\alpha$-form crystalline phase have been assigned to *trans* conformers of trimethylene group, whereas the infrared bands at 1357 and 1372 $cm^{-1}$ sensitive to PTN $\beta$-form crystalline phase have been assigned to *gauche* conformers. On the basis of FTIR results, we suggested that trimethylene glycol residue in PTN $\alpha$-form crystalline phase might adopt the G′TTG or GTTG′ conformation. We found that the PTN $\alpha$-form crystal undergoes structure change upon annealing at temperatures above 170 °C. The ATR-FTIR results showed that the bands at 1326 and 988 $cm^{-1}$ have been significantly shifted to lower wavenumbers, and new infrared bands at 1142 and 921 $cm^{-1}$ appeared upon annealing or heating of the PTN $\alpha$-form crystal at above 170 °C. The results indicated that the interaction between neighboring methylene and naphthalene groups in PTN $\alpha$-form crystalline phase was enhanced by thermal treatment. We also found that a new diffraction peak appeared upon annealing of PTN $\alpha$-form crystal. On the basis of DSC, WAXS, SAXS, and ATR-FTIR results, we concluded that: (1) The PTN $\alpha$-form crystals can transform to more stable crystalline phase (named $\alpha'$-form crystal) upon annealing or heating at above 170 °C (170−195 °C). (2) The conformation of trimethylene glycol residue in both PTN $\alpha$- and $\alpha'$-form crystals is similar to the G′TTG or GTTG′ conformation; however, the interchains interaction in PTN $\alpha'$-form crystalline phase is more stronger than that in $\alpha$-form crystalline phase. (3) The crystal changes of PTN $\alpha$-form crystal is associated with interchains rearrangement which might be caused by the surface recrystallization generated internal force.

## AUTHOR INFORMATION

### Corresponding Author

*E-mail: liangyr@bipt.edu.cn (Y.L.).

### Notes

The authors declare no competing financial interest.

## ACKNOWLEDGMENTS

This research work was partially supported by National Natural Science Foundation of China (No. 21374125) and the Importation and Development of High-Caliber Talents Project of Beijing Municipal Institutions (CIT&TCD201504048). The SAXS and WAXS experiments at PLS, Korea, were supported by MOST and POSCO, Korea. The work of crystal modeling is helped by Prof. Bin Kong from Institute of Chemistry, Chinese Academy of Sciences (ICCAS), China.

## REFERENCES

(1) Hwo, C.; Forschner, T.; Lowtan, R.; Gwyn, D.; Cristea, B. *J. Plast Film Sheet* **1999**, *15*, 219−234.
(2) Stier, U.; Oppermann, W. *J. Polym. Sci., Part A: Polym. Chem.* **2001**, *39*, 620−629.
(3) Stier, U.; Schawaller, D.; Oppermann, W. *Polymer* **2001**, *42*, 8753−8757.
(4) Stier, U.; Oppermann, W. *J. Appl. Polym. Sci.* **2002**, *84*, 2489−2497.
(5) Jeong, Y. G.; Jo, W. H.; Lee, S. C. *Polymer* **2003**, *44* (11), 3259−3267.
(6) Jeong, Y. G.; Jo, W. H.; Lee, S. C. *Polymer* **2004**, *45*, 379−384.
(7) Liang, Y.; Lee, H. S. *Macromolecules* **2005**, *38*, 9885−9888.
(8) Jeong, Y. G.; Jo, W. H.; Lee, S. C. *Polymer* **2004**, *45* (2), 379−384.
(9) Chuang, W.-T.; Hong, P.-D.; Chen, C.-H.; Sheu, H.-S.; Jeng, U.-S. *J. Appl. Crystallogr.* **2007**, *40*, s637−s641.
(10) Liang, Y.; Zheng, M.; Park, K. H.; Lee, H. S. *Polymer* **2008**, *49* (7), 1961−1967.
(11) Lee, B.; Shin, T. J.; Lee, S. W.; Yoon, J.; Kim, J.; Youn, H. S.; Ree, M. *Polymer* **2003**, *44* (8), 2509−2518.
(12) Goderis, B.; Reynaers, H.; Koch, M. H. J.; Mathot, V. B. F. *J. Polym. Sci., Part B: Polym. Phys.* **1999**, *37*, 1715−1738.
(13) Fougnies, C.; Damman, P.; Villers, D.; Dosiere, M.; Koch, M. H. J. *Macromolecules* **1997**, *30*, 1385−1391.
(14) Cebe, P.; Hsiao, B. S.; Lohse, D. J. *Sacttering from Polymers Characterization by X-rays, Neutrons, and Light*; Oxford University Press: Washington, DC, 1999.
(15) Ouchi, I.; Hosoi, M.; Shimotsuma, S. *J. Appl. Polym. Sci.* **1977**, *21*, 3445−3456.
(16) Poulin-Dandurand, S.; Pérez, S.; Revol, J.-F.; Brisse, F. *Polymer* **1979**, *20*, 419−426.
(17) Chuah, H. H. *Macromolecules* **2001**, *34*, 6985−6993.
(18) Kim, K. J.; Bae, J. H.; Kim, Y. H. *Polymer* **2001**, *42*, 1023−1033.
(19) Park, S. C.; Liang, Y.; Lee, H. S. *Macromolecules* **2004**, *37*, 5607−5614.
(20) Chiba, T.; Asai, S.; Xu, W.; Sumita, M. *J. Polym. Sci., Part B: Polym. Phys.* **1999**, *37*, 561−574.
(21) Sun, H. *J. Phys. Chem. B* **1998**, *102* (38), 7338−7364.

Downloaded by BEIJING INST PETROCHEMICAL TECHLGY on August 31, 2015 | http://pubs.acs.org
Publication Date (Web): August 14, 2015 | doi: 10.1021/acs.macromol.5b01087



DOI: 10.1021/acs.macromol.5b01087
*Macromolecules* 2015, 48, 5697−5705

(22) Ewald, P. P. *Ann. Phys.* **1921**, *64*, 253.
(23) Karasawa, N.; Goddard, W. A., III *J. Chem. Phys.* **1998**, *93* (21), 7320−7327.
(24) Kruger, K.-N.; Zachmannn, H. G. *Macromolecules* **1993**, *26*, 5202−5208.
(25) Jonas, M. M.; Russell, T. P.; Yoon, D. Y. *Macromolecules* **1995**, *28*, 8491−8503.
(26) Verma, R.; Marand, H.; Hsiao, B. *Macromolecules* **1996**, *29*, 7767−7775.
(27) Lee, B.; Shin, T. J.; Lee, S. W.; Yoon, J.; Kim, J.; Ree, M. *Macromolecules* **2004**, *37*, 4174−4184.
(28) Shimomura, M.; Iguchi, M.; Kobayashi, M. *Polymer* **1988**, *29* (2), 351−357.
(29) Tanabe, Y.; Shimomura, M. *Macromolecules* **1990**, *23*, 5031−5034.
(30) Kobayashi, M.; Sakashita, M. *J. Chem. Phys.* **1992**, *96* (1), 748−760.
(31) Kobayashi, M.; Sakashita, M.; Kobayashi, M. *Rep. Prog. Polym. Phys.* **1991**, *34*, 347.
(32) Zhang, J.; Duan, Y.; Sato, H.; Tsuji, H.; Noda, I.; Yan, S.; Ozaki, Y. *Macromolecules* **2005**, *38*, 8012−8021.
(33) Fawcett, A. H. *Polymer* **1982**, *23*, 1865.
(34) Hexter, R. M. *J. Chem. Phys.* **1960**, *33* (6), 1833−1841.
(35) Cong, Y.; Liu, H.; Wang, D.; Zhao, B.; Yan, T.; Li, L.; Chen, W.; Zhong, Z.; Lin, M.-C.; Chen, H.-L.; Yang, C. *Macromolecules* **2011**, *44*, 5878−5882.

Downloaded by BEIJING INST PETROCHEMICAL TECHLGY on August 31, 2015 | http://pubs.acs.org
Publication Date (Web): August 14, 2015 | doi: 10.1021/acs.macromol.5b01087



DOI: 10.1021/acs.macromol.5b01087
*Macromolecules* 2015, 48, 5697−5705